The Astrophysical Journal Letters, 740:L22 (6pp), 2011 October 10 doi:10.1088/2041-8205/740/1/L22

RAPID TIMESCALES FOR MAGMA OCEAN CRYSTALLIZATION ON THE HOWARDITE–EUCRITE–DIOGENITE PARENT BODY

Martin Schiller[1], Joel Baker[2], John Creech[2], Chad Paton[1],
Marc-Alban Millet[2], Anthony Irving[3], and Martin Bizzarro[1]
[1] Centre for Star and Planet Formation, Natural History Museum of Denmark, University of Copenhagen, Copenhagen DK-1350, Denmark
[2] School of Geography, Environment and Earth Sciences, Victoria University of Wellington, Wellington, New Zealand
[3] Department of Earth and Space Sciences, University of Washington, Seattle, WA 98195, USA
Received 2011 August 24; accepted 2011 September 2; published 2011 September 21

ABSTRACT

Asteroid 4 Vesta has long been postulated as the source for the howardite–eucrite–diogenite (HED) achondrite meteorites. Here we show that Al-free diogenite meteorites record variability in the mass-independent abundance of ^{26}Mg (^{26}Mg*) that is correlated with their mineral chemistry. This suggests that these meteorites captured the Mg-isotopic evolution of a large-scale differentiating magma body with increasing ^{27}Al/^{24}Mg during the lifespan of the short-lived ^{26}Al nuclide ($t_{1/2} \sim 730{,}000$ yr). Thus, diogenites and eucrites represent crystallization products of a large-scale magma ocean associated with the differentiation and magmatic evolution of the HED parent body. The ^{26}Mg* composition of the most primitive diogenites requires onset of the magma ocean crystallization within $0.6^{-0.4}_{+0.5}$ Myr of solar system formation. Moreover, ^{26}Mg* variations among diogenites and eucrites imply that near complete solidification of the HED parent body occurred within the following 2–3 Myr. Thermal models predict that such rapid cooling and magma ocean crystallization could only occur on small asteroids (<100 km), implying that 4 Vesta is not the source of the HED meteorites.

Key words: astrochemistry – meteorites, meteors, meteoroids – minor planets, asteroids: general – protoplanetary disks

1. INTRODUCTION

The accretion of nebular solids to form rocky bodies of chondritic composition, and their subsequent differentiation into asteroids or planetary embryos consisting of core, dunitic mantle, and basaltic crust, represents the initial critical steps leading to the formation of terrestrial planets. Although differentiated meteorites provide an extensive record of asteroidal melting in deep time, there is little agreement regarding the timing, nature, and extent of this igneous activity. For example, models range from small degrees of partial melting (Shearer et al. 1997) to large-scale fusion (Grove & Bartels 1992) and the formation of deep magma oceans (Righter & Drake 1997; Greenwood et al. 2005). Because the terrestrial planets grew by collisional accretion of these smaller asteroidal bodies (Chambers 2004), distinguishing between these models is essential for a better understanding of planet formation.

Given its short half-life of 730,000 yr and the contrasting geochemical behavior of the parent and daughter isotopes, the ^{26}Al-to-^{26}Mg decay system can provide a novel perspective of the timescales and mechanisms of asteroid differentiation. For example, fractional crystallization of a global magma ocean on an asteroidal body of chondritic composition will lead to the accumulation of mafic minerals such as olivine and pyroxene (^{27}Al/^{24}Mg $\sim$ 0), resulting in a progressive enhancement of the ^{27}Al/^{24}Mg ratio of the residual magma. If this process occurred during the lifespan of the ^{26}Al nuclide, ongoing crystallization would result in the formation of pyroxene and olivine with increasingly radiogenic ^{26}Mg compositions [μ^{26}Mg* = $(((^{26}\mathrm{Mg}/^{24}\mathrm{Mg})_{\mathrm{sample}}/(^{26}\mathrm{Mg}/^{24}\mathrm{Mg})_{\mathrm{standard}} - 1) \times 10^6$], which, in some cases, may exceed that of the bulk parent body. Therefore, the identification of variability in the μ^{26}Mg* values of a suite of cogenetic minerals (i.e., from a common parental magma) with ^{27}Al/^{24}Mg $\sim$ 0 is a clear fingerprint of fractional crystallization processes during the lifespan of ^{26}Al. In contrast, asteroidal differentiation may occur via variable degrees of partial melting of a chondritic parent body, directly producing melts of basaltic composition and a residual depleted mantle. In this model, mafic minerals such as olivine and pyroxene crystals that are the residues of a single-stage melt extraction event associated with asteroidal differentiation are predicted to record a homogeneous μ^{26}Mg* composition. Moreover, because Al is preferentially partitioned into the liquid phase during a melting event, partial melting residues will be characterized by a low Al/Mg ratio and, therefore, are not expected to show μ^{26}Mg* values exceeding that of their bulk parent bodies. Thus, Mg-isotope measurements of Al-poor minerals can be used to identify both the timing and mechanism(s) of asteroid differentiation, but the precision required for this approach to be fully exploited has been hitherto unattainable by state-of-the-art Mg-isotope measurements.

Diogenites are ideal samples for studying igneous processes in the early solar system because of their antiquity (Lugmair & Shukolyukov 1998) and strongly sub-chondritic ^{27}Al/^{24}Mg ratios. Diogenites are igneous, ultramafic meteorites petrogenetically associated with basaltic (i.e., eucrite) magmatism linked to the earliest stages of asteroidal melting on the howardite–eucrite–diogenite (HED) parent body, which is believed to be the asteroid 4 Vesta (Binzel & Xu 1993). Taking advantage of novel methods for the high-precision measurement of Mg-isotopes by high-resolution multiple-collector inductively coupled plasma mass spectrometry (HR-MC-ICP-MS; Bizzarro et al. 2011), we report the Mg-isotope compositions of 23 monomict diogenites with suitable precision to distinguish between models of asteroid differentiation. Our new high-precision Mg-isotope data show that Al-free diogenites record variability in their μ^{26}Mg* values that is correlated with the major- and trace-element chemistry of the coexisting pyroxene crystals. This observation establishes that initial differentiation of the HED parent body occurred through establishment of a

Table 1
Magnesium Isotope and $^{27}Al/^{24}Mg$ Data for Diogenites and Respective Mineral Compositions

Sample	$\mu^{26}Mg^*$	$\mu^{25}Mg$	$^{27}Al/^{24}Mg$		Pyroxene/Olivine	
			Sample	opx	Wo (%)	Fs (%)
NWA 1461	−10.4 ± 1.2	−120.6 ± 6.3	0.014	0.007	0.87	13.79
MET 00425	−8.4 ± 1.6	−152.4 ± 7.6	0.014	0.009	0.76	15.35
MET 00436	−8.3 ± 1.8	−127.7 ± 11.8	0.015	0.008	1.54	20.16
Bilanga	−8.0 ± 1.3	−117.0 ± 6.0	0.029	0.013	1.30	22.43
NWA 5484	−7.9 ± 1.8	−143.3 ± 8.0	0.023	0.012	1.28	21.96
MET 00855	−6.6 ± 1.5	−96.2 ± 11.9	0.015	0.008	1.39	30.80
Tatahouine	−6.2 ± 1.0	−114.7 ± 3.3	0.008	0.019	1.59	21.10
LAP 91900	−5.8 ± 2.0	−129.6 ± 8.3	0.023	0.017	1.96	24.91
MET 00422	−4.9 ± 1.7	−110.8 ± 8.6	0.019	0.012	1.53	27.39
LAP 03630	−4.6 ± 1.6	−154.4 ± 7.4	0.024	0.018	2.06	25.18
NWA 2286	−3.1 ± 1.3	−98.3 ± 9.5	0.033	0.020	2.50	21.08
MET 001060	−2.8 ± 1.5	−49.6 ± 7.6	0.012	0.009	1.09	20.99
NWA 1877	−1.6 ± 1.0	−153.0 ± 4.3	0.018	0.011	1.92	26.01
GRO 95555	+2.6 ± 2.0	−125.9 ± 19.4	0.044	0.030	2.42	24.46
Ibbenbueren	+4.7 ± 1.4	−109.5 ± 5.4	0.030	0.008	2.45	23.47
PCA 91077	+6.3 ± 1.7	−142.0 ± 5.7	0.029	0.020	2.42	26.43
NWA 1821	+11.7 ± 1.6	−111.0 ± 7.5	0.028	0.031	3.41	27.06
LEW 88008	+12.8 ± 1.8	−162.1 ± 5.5	0.091	0.038	3.56	30.61
NWA 5480	+0.7 ± 2.1	−110.0 ± 3.2	0.024	powder	Fo (%)	Fa (%)
NWA 3329	−10.8 ± 1.8	−119.3 ± 8.2	0.007	n.a.	90.96	8.79
NWA 5312	−7.0 ± 2.0	−58.8 ± 12.3	0.053	n.a.	74.76	24.68
NWA 2048	+0.1 ± 1.7	−99.0 ± 4.3	0.024	n.a.	72.36	26.99
NWA 4223	+10.1 ± 1.0	−114.7 ± 3.3	0.013	n.a.	70.08	29.15

Notes. Wo: wollastonite; Fs: ferrosilite; Fo: fosterite; Fa: fayalite; n.a.: not applicable; opx: orthopyroxene.

global magma ocean rather than partial melting of a solid silicate mantle. The observed range of $\mu^{26}Mg^*$ values among diogenite and eucrite meteorites requires that magma ocean crystallization and nearly complete solidification of the HED parent body occurred within 3–4 Myr of solar system formation.

2. METHODS

Diogenite samples selected for study were gently crushed in order to extract fragments suitable for in situ elemental analysis as well as bulk Mg-isotope measurements. The major- and trace-element compositions of minerals from the prepared diogenite fragments (mounted in epoxy and polished) were determined at Victoria University of Wellington using a JEOL JXA-8230 Superprobe electron microprobe (major elements) and an Agilent 7500CS ICP-MS coupled to a New Wave deep (193 nm) UV laser (trace elements). Electron microprobe analyses were carried out using an accelerating voltage of 15 kV, a beam current of 12 nA, and a focused beam (spot <0.5 μm). X-ray intensities were calibrated against elemental concentrations by analysis of the standards Johnstown hypersthene (Cr, Mg, Si, Al, Fe), Kakanui augite (Ti, Na, Ca), and synthetic MnO (Mn). Three secondary standards, Johnstown hypersthene (USNM 746), Kakanui augite (NMNH 122142), and Natural Bridge diopside (NMNH 117733), were repeatedly analyzed throughout the sessions as secondary standards (Jarosewich et al. 1980). Trace elements were measured by laser ablation on the same mount close to the electron microprobe pits. Each sample was analyzed 5–11 times and consisted of a ca. 60 s background measurement and 60 s (around 50 scans) of data acquisition while ablating the sample. Sample analyses were bracketed every five analyses by a measurement of the calibration standard (BCR-2G). All data treatment was performed using the "trace element IS" data reduction scheme of the Iolite software package (Paton et al. 2011). The background-corrected data were converted to absolute element concentrations using ^{29}Si for internal element normalization and using the element concentrations in the BCR-2 glass standard (GeoRem 2010) and the silicon concentrations previously determined by electron microprobe.

Fragments weighing between 10 and 150 mg were selected for Mg-isotope measurements and crushed to a fine powder with an agate mortar for acid digestion with HF-HNO_3 mixtures in Teflon beakers on a hot plate at 150°C. After complete dissolution, samples were processed following the procedure described in Bizzarro et al. (2011) for Mg purification. Mg isotopes and $^{27}Al/^{24}Mg$ ratios were measured with a Thermo Finnigan Neptune multiple-collector inductively coupled plasma mass spectrometer (MC-ICP-MS) at the Centre for Star and Planet Formation (University of Copenhagen) following techniques described in Bizzarro et al. (2011). The external reproducibility of $\mu^{26}Mg^*$ is estimated to be ±2.5 ppm (parts per million) using the described analytical conditions based on repeated analyses of various standards (Bizzarro et al. 2011).

3. RESULTS

Our new Mg-isotope data and major mineral data are reported in Tables 1 and 2. The diogenite samples we selected for this study comprise orthopyroxene and olivine with compositions ranging from En = 65.8–85.3 mol% and Fo = 70.1–91.0 mol%, respectively, encompassing the known range of compositional variability for this class of meteorites. $^{27}Al/^{24}Mg$ ratios in the bulk sample digestions range from 0.007 to 0.053 and overlap with $^{27}Al/^{24}Mg$ ratios measured in situ in coexisting pyroxenes (0.007–0.038). The bulk sample digestions of diogenites record $\mu^{26}Mg^*$ values that vary from −10.8 ± 1.8 to +12.8 ± 1.8 ppm (Figure 1(A), Table 1). Minor incompatible element concentrations in pyroxenes such as Ca and Mn show large

Table 2
Major- and Trace-element Concentrations of Diogenite Pyroxene

Sample	SiO_2 (wt.%)	TiO_2 (wt.%)	Al_2O_3 (wt.%)	Cr_2O_3 (wt.%)	FeO (wt.%)	MnO (wt.%)	MgO (wt.%)	CaO (wt.%)	Na_2O (wt.%)	Sc (ppm)	V (ppm)	Co (ppm)	Ni (ppm)	Cu (ppm)	Zn (ppm)	Sr (ppm)	Y (ppm)
NWA 1461	56.01	0.031	0.31	0.69	9.43	0.35	32.78	0.47	0.01	12.12	76.5	10	5.07	n.d.	1.098	0.988	0.237
MET 00425	55.84	0.026	0.41	0.62	10.83	0.36	28.93	0.36	0.01	12.66	73.9	11.5	5.25	0.24	1.286	0.258	0.167
MET 00436	53.57	0.025	0.28	0.18	18.77	0.68	23.61	0.65	0	17.76	82.9	3.5	0.1	0.042	1.07	0.223	0.15
Bilanga	54.91	0.068	0.53	0.6	14.81	0.42	28.25	0.67	0	18.36	89.5	16.1	2.64	0.301	1.03	0.119	0.757
NWA 5484	54.84	0.036	0.52	0.43	14.74	0.55	29.08	0.68	0	19.91	95.5	11.5	0.36	0.721	1.207	0.452	0.376
MET 00855	53.42	0.024	0.31	0.18	18.94	0.68	23.39	0.67	0	17	82.2	5.1	0.13	0.468	1.114	0.198	0.226
Tatahouine	53.15	0.065	0.8	0.71	12.8	0.48	26.34	0.75	0.01	18.88	103.3	11.6	7.41	0.245	0.778	0.018	0.247
LAP 91900	53.63	0.054	0.63	0.67	15.44	0.55	25.5	0.95	0.01	15.5	100.7	10.7	4	0.17	0.906	0.154	0.447
MET 00422	53.92	0.039	0.47	0.7	16.95	0.59	24.67	0.73	0.01	12.65	105.9	15.2	9.77	1.267	1.348	0.124	0.176
LAP 03630	53.5	0.059	0.68	0.63	15.57	0.54	25.17	1	0.01	15.65	97.9	10.8	1.72	0.056	1.145	0.131	0.551
NWA 2286	54.07	0.034	0.78	0.28	15.95	0.57	26.93	0.64	0.01	18.51	112.7	7.5	0.64	0.687	0.932	0.262	0.119
MET 001060	55.23	0.045	0.39	0.29	13.35	0.54	27.85	0.54	0	14.22	97.8	2.5	0.55	0.103	1.227	0.079	0.12
NWA 1877	54.23	0.054	0.39	0.4	16.78	0.6	26.03	0.96	0.01	21.01	141.3	5.7	0.27	0.081	1.144	0.214	0.338
GRO 95555	53.44	0.082	1.12	0.82	14.91	0.55	25	1.15	0.02	14.82	123.2	8.6	0.64	n.d.	1.209	0.249	0.986
Ibbenbueren	53.02	0.101	0.32	0.32	14.94	0.51	26.4	1.22	0.01	19.74	82.8	16.9	12.96	n.d.	1.284	0.142	1.203
PCA 91077	53.97	0.082	0.74	0.69	16.35	0.59	24.69	1.17	0.01	15.99	102	13	9.28	0.42	0.968	0.214	0.89
NWA 1821	53.41	0.117	1.13	0.74	16.92	0.63	22.29	1.68	0.01	20.22	114.4	11.3	7.43	0.543	1.369	0.356	1.397
LEW 88008	52.24	0.138	1.25	0.89	18.48	0.59	24.46	1.67	0.01	26.61	152.4	11.5	1.54	0.04	0.801	0.027	1.628

Sample	Zr (ppm)	Nb (ppm)	La (ppm)	Ce (ppm)	Pr (ppm)	Nd (ppm)	Sm (ppm)	Eu (ppm)	Gd (ppm)	Tb (ppm)	Dy (ppm)	Ho (ppm)	Er (ppm)	Tm (ppm)	Yb (ppm)	Lu (ppm)	Hf (ppm)
NWA 1461	0.266	0.018	0.017	0.114	0.016	0.099	0.021	0.009	0.028	0.001	0.021	0.005	0.033	0.004	0.033	0.011	0.009
MET 00425	0.633	0.052	0.022	0.092	0.015	0.077	0.033	0.004	0.039	0.005	0.031	0.005	0.016	0.003	0.019	0.005	0.012
MET 00436	0.205	0.004	0	0.011	0.002	0.02	0.017	0.001	0.021	0.002	0.02	0.004	0.014	0.002	0.019	0.003	0.006
Bilanga	0.724	0.203	0.011	0.037	0.006	0.04	0.03	0.006	0.07	0.012	0.124	0.027	0.082	0.015	0.112	0.02	0.023
NWA 5484	0.194	0.016	0.006	0.007	0.002	0.01	0.002	0	0.019	0.007	0.056	0.009	0.039	0.01	0.051	0.01	0.022
MET 00855	0.304	0.006	0.006	0.02	0.004	0.027	0.012	0.002	0.021	0.004	0.032	0.007	0.024	0.004	0.023	0.005	0.006
Tatahouine	0.025	0.016	0	0.002	0.001	n.d.	n.d.	n.d.	0.001	0.004	0.03	0.009	0.046	0.012	0.072	0.013	0.001
LAP 91900	0.386	0.022	0.004	0.018	0.005	0.029	0.012	0	0.03	0.008	0.054	0.015	0.053	0.01	0.076	0.014	0.011
MET 00422	0.168	0.019	0.007	0.027	0.004	0.016	0.006	0.001	0.015	0.002	0.025	0.005	0.023	0.006	0.028	0.006	0.006
LAP 03630	0.363	0.012	0.003	0.016	0.004	0.023	0.024	0.002	0.026	0.006	0.074	0.019	0.069	0.011	0.098	0.017	0.01
NWA 2286	0.038	0.012	0.001	0.011	0.005	0.019	n.d.	n.d.	n.d.	0.002	0.018	0.005	0.02	0.005	0.034	0.004	n.d.
MET 001060	0.018	0.014	0.002	0.015	0.002	0.017	0.003	n.d.	0.003	0	0.011	0.004	0.022	0.003	0.039	0.008	0.003
NWA 1877	0.727	0.016	0.004	0.02	0.008	0.05	0.031	0.008	0.04	0.01	0.043	0.011	0.047	0.005	0.074	0.01	0.041
GRO 95555	2.415	0.025	0.023	0.166	0.035	0.264	0.075	0.011	0.114	0.021	0.153	0.037	0.122	0.019	0.138	0.022	0.07
Ibbenbueren	0.703	0.017	n.d.	0.017	0.004	0.043	0.025	n.d.	0.085	0.02	0.171	0.05	0.139	0.028	0.171	0.035	0.026
PCA 91077	0.617	0.017	0.006	0.033	0.006	0.049	0.02	0.007	0.057	0.015	0.121	0.03	0.108	0.02	0.143	0.024	0.022
NWA 1821	1.12	0.02	0.021	0.154	0.014	0.094	0.051	0.003	0.113	0.024	0.205	0.05	0.167	0.03	0.227	0.041	0.039
LEW 88008	0.469	0.018	0.005	0.008	0.002	0.021	0.014	0.002	0.071	0.018	0.181	0.05	0.21	0.033	0.265	0.047	0.02

Note. n.d.: not detected.

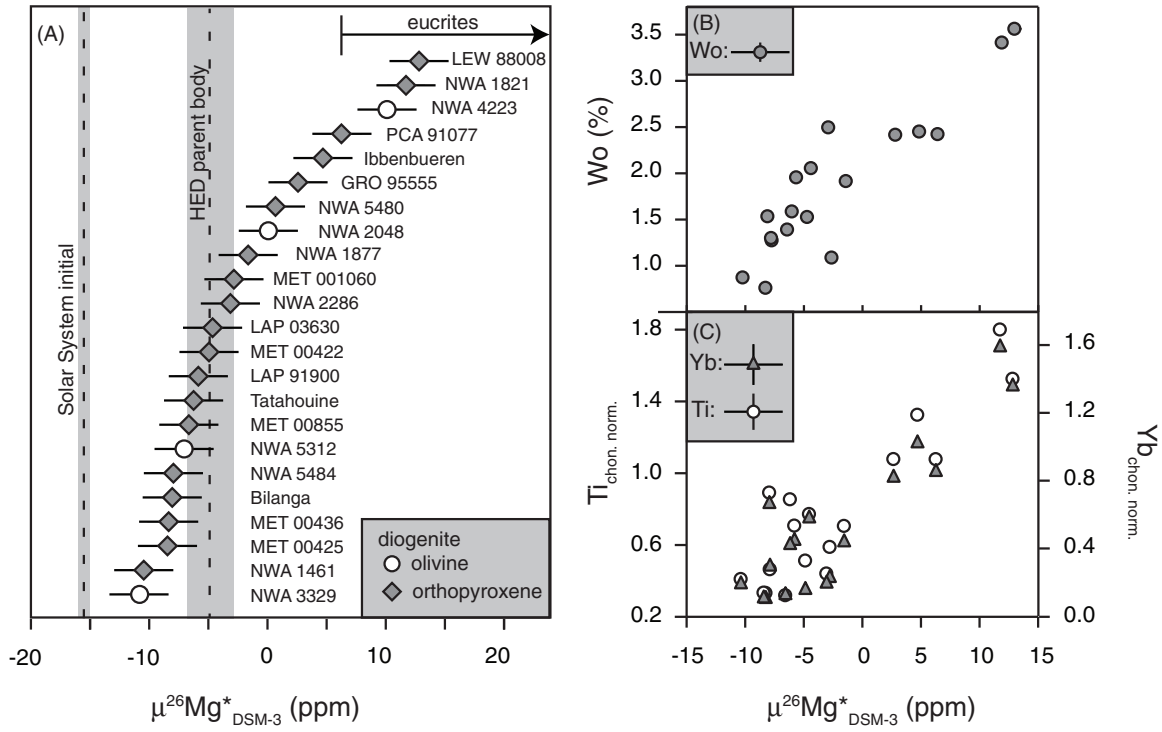

Figure 1. (A) μ^{26}Mg* values for bulk diogenites. The range of eucrite μ^{26}Mg* values shown is based on data from Bizzarro et al. (2005) and Schiller et al. (2010). Also shown is the initial solar system's μ^{26}Mg* value (Larsen et al. 2011) as well as the HED parent body bulk μ^{26}Mg* composition after complete decay of ^{26}Al (see the text). Plotted uncertainties represent the external reproducibility of 2.5 ppm. The wollastonite (Ca) content in orthopyroxene (A) and the average CI chondrite-normalized (Palme & Jones 2003) Ti and Yb concentrations in orthopyroxene (B) are plotted against the μ^{26}Mg* values for bulk diogenites.

variations in their absolute concentrations (Table 2) that are reversely correlated with the En component of the pyroxene. Trace elements and especially heavy rare earth element (REE) concentrations in diogenite pyroxene show a range in absolute concentrations that spans an order of magnitude. The variability in concentrations of both minor and incompatible trace elements is positively correlated with μ^{26}Mg* values of the respective diogenite samples (Figures 1(B) and (C)).

4. DISCUSSION

The μ^{26}Mg* variability in diogenites is not correlated to exposure ages of the individual samples (Welten et al. 1997) or the stable Mg-isotope composition of the individual samples. Thus it cannot be explained by cosmogenic processes or inappropriate instrumental mass bias corrections (Bizzarro et al. 2011). Contamination of primitive diogenites having uniform μ^{26}Mg* with variable amounts of eucritic material as the source of the diogenite μ^{26}Mg* variability is unlikely, given that the very large degree of contamination required (>50%) to explain the observed range of diogenite μ^{26}Mg* values would have altered the major-element chemistry of the affected diogenites. In contrast, the variations in μ^{26}Mg* for diogenites are positively correlated with the major-element and incompatible trace-element concentrations (e.g., REE) of orthopyroxene crystals (Figures 1(B) and (C)), thereby supporting the idea that diogenite meteorites are part of a cogenetic magmatic suite (Warren & Jerde 1987). Some of the diogenites in this correlation have μ^{26}Mg* values that are higher than the bulk parent body μ^{26}Mg* after complete decay of ^{26}Al. This observation is not consistent with diogenite formation by melt extraction but requires diogenites to have inherited their μ^{26}Mg* values from an evolving parent magma with elevated ^{27}Al/^{24}Mg ratios. Therefore, we infer that the variability in the μ^{26}Mg* values of diogenites tracks the isotopic evolution of a large-scale differentiating magma body with evolving ^{27}Al/^{24}Mg ratios while ^{26}Al was extant. The diogenite samples NWA 1461 and NWA 3329, interpreted as representing the earliest cumulates based on their high Mg numbers [Mg/(Mg+Fe)×100], record the largest deficits in μ^{26}Mg*, whereas samples with low Mg numbers—interpreted to reflect later cumulates—are characterized by the greatest excesses in μ^{26}Mg*. Based on the increase in heavy REE concentrations in the orthopyroxene crystals from the earliest (NWA 1461) to the latest (LEW 88008) cumulate phase (Table 2) and assuming a constant distribution coefficient between melt and orthopyroxene (van Kan Parker et al. 2010), we conservatively estimate that the range of diogenite compositions we sampled requires at least 50%–75% fractional crystallization of the parental magma, in agreement with an earlier study (Grove & Bartels 1992). Thus, our results indicate that diogenite meteorites represent crystallization products of a large-scale magma ocean associated with the initial differentiation and extensive magmatic evolution of the HED parent body.

In contrast to our interpretation, we note that earlier studies (Barrat et al. 2008, 2010) have proposed that diogenite meteorites represent crystallization products of multiple small magmatic chambers within the HED, based on the observation of significant variability in their REE and trace-element chemistry. However, these data were obtained on whole-rock analyses and, as such, are not immune to potential biases related to the presence of a trapped, interstitial melt component. Although it is not possible to rule out the presence of multiple small magma chambers on the HED parent body based on our data, the simple correlation between the μ^{26}Mg* of bulk diogenites and the chemistry of their coexisting pyroxene crystals would imply

that the diogenite suite we studied represents samples of a single magmatic chamber or, alternatively, of multiple chambers with nearly identical chemical evolutions. Thus, we infer that the most straightforward interpretation of our data is that diogenite meteorites represent samples of a large-scale differentiating magma ocean.

Constraining the onset and duration of magma ocean crystallization on the HED parent body requires knowledge of the initial abundance of ^{26}Al in the accretion region of the HED parent body, as well as the rate of change of the ^{27}Al/^{24}Mg ratio in the crystallizing magma ocean. A recent high-precision Mg-isotope study (Larsen et al. 2011) of inner solar system solids, asteroids, and planetary bodies suggests that large-scale heterogeneity in the initial abundance of ^{26}Al may have existed in the protoplanetary disk at the time of formation of the solar system's first solids, calcium-aluminum-rich inclusions (CAIs). The inferred variations in the initial abundance of ^{26}Al correlate with the ^{54}Cr/^{52}Cr ratios for the same reservoirs and, therefore, we used the inner solar system ϵ^{54}Cr–μ^{26}Mg* relationship (Larsen et al. 2011) to estimate an initial ^{26}Al/^{27}Al ratio of $(1.6 \pm 0.3) \times 10^{-5}$ for the HED parent body. After complete decay of ^{26}Al, this equates to a bulk present-day μ^{26}Mg* value of -4.9 ± 2.0 ppm for the HED parent body, assuming that it formed with a solar ^{27}Al/^{24}Mg ratio of 0.101 (Palme & Jones 2003). Using the bulk μ^{26}Mg* value for the HED parent body, it is possible to calculate a model isochron for the crystallization age of the two most primitive diogenite samples, NWA 1461 and NWA 3329, which are interpreted as representing the earliest preserved cumulate phases based on their mineral chemistry and lowest μ^{26}Mg* values. Thus, their crystallization ages provide a conservative estimate for the formation and onset of crystallization of the HED magma ocean. The resulting $(^{26}\mathrm{Al}/^{27}\mathrm{Al})_0$ value of the model isochron using the NWA 1461 and NWA 3329 diogenites corresponds to a relative age of $0.6^{-0.4}_{+0.5}$ Myr after condensation of CAIs, which represents our best estimate for the onset of magma ocean crystallization on the HED.

That diogenite meteorites represent initial crystallization products of a large-scale magma ocean associated with an early and global asteroidal melting event is consistent with the idea that eucrites represent late-stage products of the residual liquid (Ruzicka et al. 1997). In this view, diogenites, most basaltic eucrites and cumulate eucrites, formed as part of a simple and continuous crystallization sequence. The duration of this crystallization sequence can be estimated by reconstructing the rate of ingrowth of the μ^{26}Mg* value, which is controlled by a sustained increase in the ^{27}Al/^{24}Mg ratio of the magma ocean as a result of fractional crystallization processes. Because basaltic and cumulate eucrites are late-stage products of the crystallization sequence, their bulk μ^{26}Mg* values can be used to estimate the final composition of the magma ocean prior to solidification. We focus our discussion on the Juvinas and Dhofar 007 basaltic and cumulate eucrites, respectively, as their bulk μ^{26}Mg* values have been measured to high precision by two different studies (Bizzarro et al. 2005; Schiller et al. 2010). Using the bulk μ^{26}Mg* value of the most primitive diogenite (NWA 3329) as an estimate of the initial composition of the magma ocean, we show in Figure 2 that it is possible to model the μ^{26}Mg* values of the Juvinas and Dhofar 007 eucrites using an exponential rate of change of the ^{27}Al/^{24}Mg ratio in the magma ocean. This approach constrains the duration of the entire crystallization sequence of the diogenite samples to within 2.5 Myr of CAI condensation, and the formation of the cumulate and basaltic eucrite reservoirs at 2.1 and 2.8 Myr, respectively.

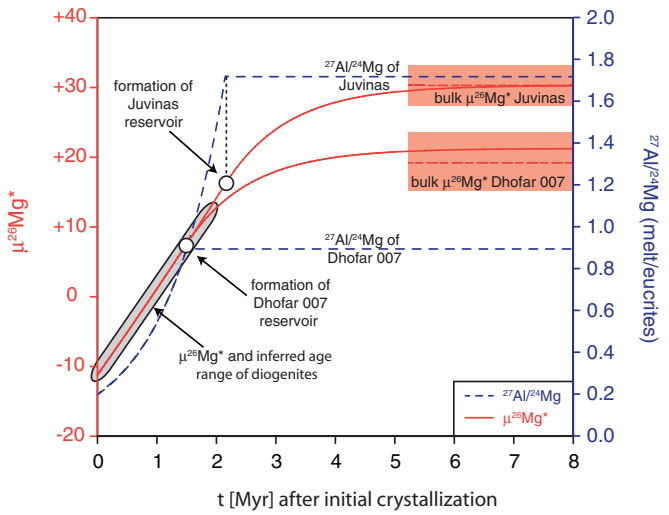

Figure 2. Modeled time evolution of the μ^{26}Mg* composition of a crystallizing magma ocean based on an exponential rate of change for the ^{27}Al/^{24}Mg ratio. The initial ^{27}Al/^{24}Mg ratio of the magma ocean was assumed to be 0.2 in order to reflect 50% partial melting of a chondritic body with a solar ^{27}Al/^{24}Mg ratio. The timing of extraction and the final μ^{26}Mg* composition of hypothetical cumulate and basaltic eucrite reservoirs with ^{27}Al/^{24}Mg ratios of 0.9 and 1.7, respectively, are indicated. The final μ^{26}Mg* compositions of these two reservoirs are in good agreement with those observed for the Dhofar 007 (^{27}Al/^{24}Mg = 0.9) and Juvinas (^{27}Al/^{24}Mg = 1.7) cumulate and basaltic eucrites. Also shown is the range of μ^{26}Mg* values measured in diogenites and their resulting age range.

These rapid timescales for the magmatic evolution of the HED inferred from our data are consistent with the timing of crust, mantle, and core formation suggested by ^{53}Mn–^{53}Cr and ^{182}Hf–^{182}W systematics of eucrite meteorites (Trinquier et al. 2008; Kleine et al. 2009). We note that the μ^{26}Mg* value of the last diogenite to crystallize prior to the extraction of the eucrite reservoirs predicted by the model based on an exponential rate of change of the ^{27}Al/^{24}Mg ratio in the magma ocean is ~+8 ppm. Considering the uncertainty associated with this model and our isotope measurements, this value compares favorably with the μ^{26}Mg* value of 12.8 ± 2.5 ppm obtained for the most evolved diogenite sample (LEW 88008). This observation gives further credence to our proposal that diogenites, and most basaltic eucrites and cumulate eucrites, are products of a simple and continuous crystallization trend on the HED parent body.

Our revised chronology for the formation of diogenite and eucrite meteorites suggests that magma ocean crystallization on the HED parent body began within ~1 Myr of solar system formation and its near complete solidification occurred within the following 3 Myr. Such timescales require that effective cooling of the parent body was initiated very shortly after global melting. Currently, the source of the HED meteorite suite is believed to be asteroid 4 Vesta—a ~530 km diameter differentiated body located in the inner part of the asteroid belt—based on similarities in reflectance spectra (Binzel & Xu 1993; Gaffey 1997). Studies modeling the thermal history of a Vesta-like asteroid heated by the radioactive decay of ^{26}Al require timescales of >10 Myr for the cooling and crystallization of a global magma ocean (Ghosh & McSween 1998; Hevey & Sanders 2006; Gupta & Sahijpal 2010), even when allowing for a reduced initial abundance of ^{26}Al in the source region of this asteroid (Larsen et al. 2011, Figure 3(a)). This extended magmatic history is not consistent with the timing of magma ocean crystallization on the HED parent body inferred from

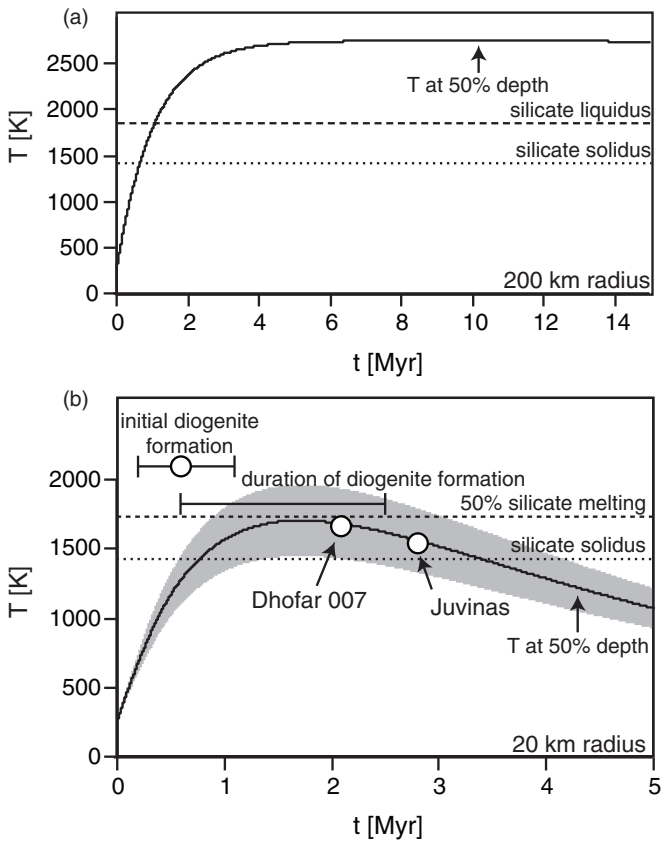

Figure 3. Thermal evolution models using conductive heat transfer for (a) 200 km radius (Vesta-like) and (b) 20 km radius asteroidal bodies. Ages shown in (b) for diogenites and eucrites are from Figure 2 and a model isochron for the onset of diogenite formation (see the text). The gray area in (b) reflects the model uncertainty associated with the uncertainty in $(^{26}Al/^{27}Al)_0$ of the HED parent body. Solidus–liquidus lines are based on Taylor et al. (1993). Apart from radius, the physical parameters used in each model are identical. The model calculations are based on a numerical solution of the equation of heat conduction using a one-dimensional model with rotational symmetry (using Equation (1) of Hevey & Sanders 2006). The model contains radial loss due to sintering, shrinking radius sections to 77% of their initial size when temperatures exceed 700 K. Unsintered sections have a thermal conductivity that is reduced by a factor of 1000. Instantaneous asteroid accretion at $T = 0$ was assumed. Energy production is based on an initial $^{26}Al = 1.55 \times 10^{-5}$ and 3.12 MeV decay energy and an Al abundance of 1.2 wt.% (Larsen et al. 2011; Castillo-Rogez et al. 2009; Kallemeyn et al. 1989). Values for density (3300 kg m^{-3}) and thermal conductivity (2.1 W m^{-1}) were taken from Hevey & Sanders (2006), and the specific heat capacity (800 J kg^{-1} K^{-1}) is based on Ghosh & McSween (1999). Time steps were in 100 years and radial sections have a 1% thickness of the total radius.

our Mg-isotope measurements of diogenite meteorites, implying that 4 Vesta may not be the source of HED meteorites. Rather, the rapid timescales we propose are consistent with an asteroidal body characterized by a diameter of <100 km as the source of the HED meteorites (Figure 3(b)).

In anticipation of results from the *Dawn* mission to asteroid 4 Vesta, a better understanding of the expected composition of 4 Vesta's crust is timely. Thus, a central question emerging from our results and interpretation is whether any of the meteorites currently in our collections are, indeed, derived from 4 Vesta. A total of seven anomalous eucrite-like basaltic meteorites have been identified based on their mass-independent oxygen isotope compositions (Scott et al. 2009; Bland et al. 2009), which suggests that they may have formed on parent asteroids distinct from the HED parent body. However, the major-element chemistry of these anomalous basaltic meteorites is compatible with a petrogenetic history similar to basalts from the HED suite, namely, as late-stage products of a differentiating magma ocean. We note that two of these basaltic meteorites, Ibitira and NWA 011, have small bulk $\mu^{26}Mg^*$ excesses similar to those observed in typical eucrite meteorites (Bizzarro et al. 2005; Schiller et al. 2010), indicative of a rapid magmatic evolution of their parent bodies and, therefore, are also not likely to be derived from 4 Vesta. Thus, a hallmark of meteorites originating from large differentiated asteroids like 4 Vesta may be the lack of evidence for the former presence of short-lived radionuclides such as ^{26}Al, given the protracted magmatic history of a differentiating magma ocean inferred from thermal modeling of such asteroidal bodies.

Financial support for this project was provided by the Centre for Star and Planet Formation and New Zealand's Marsden Fund. The Centre for Star and Planet Formation is financed by the Danish National Science Foundation.

REFERENCES

Barrat, J.-A., Yamaguchi, A., Greenwood, R. C., et al. 2008, Meteorit. Planet. Sci., 43, 1159
Barrat, J.-A., Yamaguchi, A., Zanda, B., Bollinger, C., & Bohn, M. 2010, Geochim. Cosmochim. Acta, 74, 628
Binzel, R., & Xu, S. 1993, Science, 260, 186
Bizzarro, M., Baker, J. A., Haack, H., & Lundgaard, K. 2005, ApJ, 632, L42
Bizzarro, M., Paton, C., Larsen, K., et al. 2011, J. Anal. At. Spectrom., 26, 565
Bland, P. A., Spurný, P., Towner, M. C., et al. 2009, Science, 325, 1525
Castillo-Rogez, J., Johnson, T., Lee, M., et al. 2009, Icarus, 204, 658
Chambers, J. E. 2004, Earth Planet. Sci. Lett., 223, 241
Gaffey, M. 1997, Icarus, 127, 130
GeoRem. 2010, http://georem.mpch-mainz.gwdg.de/
Ghosh, A., & McSween, H. 1998, Icarus, 134, 187
Ghosh, A., & McSween, H. 1999, Meteorit. Planet. Sci., 34, 121
Greenwood, R., Franchi, I., Jambon, A., & Buchanan, P. 2005, Nature, 435, 916
Grove, T., & Bartels, K. 1992, in Proc. Lunar and Planetary Science, 22, 437
Gupta, G., & Sahijpal, S. 2010, J. Geophys. Res., 115, E08001
Hevey, P., & Sanders, I. 2006, Meteorit. Planet. Sci., 41, 95
Jarosewich, E., Nelen, J., & Norberg, J. 1980, Geostandard Newslett., 4, 43
Kallemeyn, G. W., Rubin, A. E., Wang, D., & Wasson, J. T. 1989, Geochim. Cosmochim. Acta, 53, 2747
Kleine, T., Touboul, M., Bourdon, B., et al. 2009, Geochim. Cosmochim. Acta, 73, 5150
Larsen, K. K., Trinquier, A., Paton, C., et al. 2011, ApJ, 735, L37
Lugmair, G., & Shukolyukov, A. 1998, Geochim. Cosmochim. Acta, 62, 2863
Palme, H., & Jones, A. 2003, in Treatise on Geochemistry, Vol. 1, ed. A. W. Davis (Oxford: Elsevier), 41
Paton, C., Hellstrom, J., Paul, B., Woodhead, J., & Hergt, J. 2011, J. Anal. At. Spectrom.
Righter, K., & Drake, M. 1997, Meteorit. Planet. Sci., 32, 929
Ruzicka, A., Snyder, G., & Taylor, L. 1997, Meteorit. Planet. Sci., 32, 825
Schiller, M., Baker, J. A., & Bizzarro, M. 2010, Geochim. Cosmochim. Acta, 74, 4844
Scott, E. R. D., Greenwood, R. C., Franchi, I. A., & Sanders, I. S. 2009, Geochim. Cosmochim. Acta, 73, 5835
Shearer, C., Fowler, G., & Papike, J. 1997, Meteorit. Planet. Sci., 32, 877
Taylor, G., Keil, K., McCoy, T., Haack, H., & Scott, E. 1993, Meteoritics, 28, 34
Trinquier, A., Birck, J.-L., Allegre, C., Göpel, C., & Ulfbeck, D. 2008, Geochim. Cosmochim. Acta, 72, 5146
van Kan Parker, M., Liebscher, A., Frei, D., et al. 2010, Contrib. Mineral. Petrol., 159, 459
Warren, P., & Jerde, E. 1987, Geochim. Cosmochim. Acta, 51, 713
Welten, K., Lindner, L., van der Borg, K., et al. 1997, Meteorit. Planet. Sci., 32, 891